Four wave mixing in 3C SiC Ring Resonators

Francesco Martini[1] and Alberto Politi[1, a)]
Department of Physics and Astronomy, University of Southampton, Southampton, SO17 1BJ, UK

We demonstrate frequency conversion by four wave mixing at telecommunication wavelengths using an integrated platform in 3C SiC. The process was enhanced by high-Q and small modal volume ring resonators, allowing the use of mW-level CW powers to pump the nonlinear optical process. From this measurement we retrieved the nonlinear refractive index of 3C SiC as $n_2 = (5.31 \pm 0.04) \times 10^{-19} m^2/W$.

Third order nonlinear effects are relevant for a broad variety of optical process in integrated structures, ranging from wavelength conversion[1–3], amplification[4] and self phase modulation[5] to generation of non-classical state of light[6]. These effects were widely studied in Silicon (Si)[7], due to its high $\chi^{(3)}$ susceptibility and scalability, and Silicon Nitride[8] (Si_3N_4), due to its low propagation loss and wide bandgap. Recently, photonic platforms in Aluminium Nitride[9] and Diamond[10] have reached competitive results. However, the development of quantum technologies has risen interest in new materials that are able to integrate different capabilities[11], like the presence of quantum emitters[12] and a non-centrosymmetric crystalline structure[13]. In addition to meet these requirements, Silicon Carbide (SiC) offers a wide bandgap (2.3 eV), a high refractive index (2.6) and high-quality layers are commercially available. Between all the different polytypes, cubic SiC (3C SiC) can be grown heteroepitaxially on top of Si substrates, reducing the fabrication steps required to fabricate integrated structures. Recently, $\chi^{(3)}$ effects were demonstrated in amorphous[14] SiC toroids at telecommunication wavelengths[15] and in 4H SiC waveguides in the mid infrared wavelengths[16]. Even though numerical predictions are available for 3C SiC $\chi^{(3)}$ susceptibility[17], third order nonlinear effects have not been experimentally demonstrated due to difficulties in fabricating sub-μm photonic devices. Recently, we demonstrated high confinement optical components in suspended 3C SiC[18], suitable for exploring optical nonlinearities.

In this letter we report the demonstration of frequency conversion by four-wave mixing (FWM) in 3C SiC ring resonators, fully integrated in an optical circuit composed of grating couplers, bus waveguides and mode converters. We achieved a conversion efficiency of $-72dB$ at the low pump power of $2.9mW$. The absence of two photon absorption at telecom wavelength does not limit the pump intensity, meaning that high conversion efficiencies are possible. The retrieved nonlinear refractive index $n_2 = (5.31 \pm 0.04) 10^{-19} m^2/W$ is almost twice the value of Si_3N_4 and comparable to many materials used for nonlinear photonics.

Optical nonlinearities can be enhanced by decreasing the cross-section of waveguides[19], in which the small mode area A_{eff} increases the effective nonlinearity γ of structures

$$\gamma = \frac{n_2 \omega_p}{A_{eff} c} \tag{1}$$

where ω_p is the pump frequency and c is the speed of light in vacuum. Thanks to the tight confinement, efficient frequency conversion can be demonstrated using millimeter long high-confinement waveguides together with a broad conversion bandwidth[3], provided anomalous group velocity dispersion (GVD) is obtained for the structures.

Further improvements in both conversion efficiency and footprint of devices can be achieved using cavity structures, including ring resonators[2]. When the frequency of light is resonant with the cavity, the intensity of the electromagnetic field is enhanced, increasing the conversion efficiency of the nonlinear process. For a resonator of length L and propagation losses α, the field enhancement (FE) is dependent by the field coupling from the bus waveguide to the ring σ, and the transmitted field through the bus waveguide τ (with $\sigma^2 + \tau^2 = 1$), by

$$FE = \left| \frac{\sigma}{1 - \tau \exp(-\alpha L/2 + jkL)} \right| \tag{2}$$

where k is the wavenumber. The maximum value of FE is reached when the field wavelength is resonant with the cavity ($kL = 2m\pi$, with m integer) and the resonator is in critical coupling condition ($a = \tau$). Satisfied the previous conditions and in the ideal case of $\sigma << 1$ (low loss regime), the FE can be linked directly to the quality factor (Q) of the cavity

$$FE = \sqrt{\frac{2Q}{k_p L}} \tag{3}$$

By looking at Eq.1 and 3, an increase in the Q factor and a reduction in the modal volume of the resonator correspond to the enhancement of the field inside the photonic structure, providing increased FWM efficiency.

The SiC device used for FWM experiments was fabricated using two steps of electron beam lithography to define waveguides suspended in air, as reported in our previous work[18]. The device includes waveguides composed by a $\sim 730 \times 500nm$ structure on top on a $200nm$-thick membrane, resulting in multi-mode operation at telecom wavelength and rings resonators of radius $10\mu m$. Even

a) A.Politi@soton.ac.uk

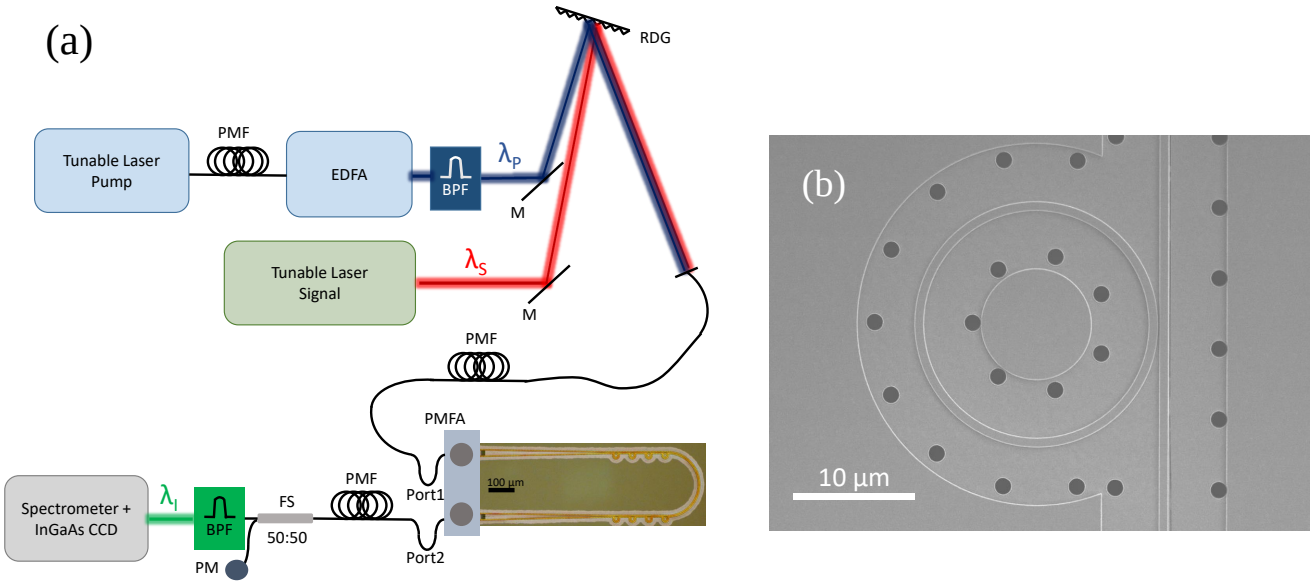

FIG. 1. a) Experimental setup for the characterization of the FWM process, including an optical micrograph of the sample. PMF, Polarization Maintaining Fiber; EDFA, Erbium-Doped Fiber Amplifier; BPF, Band Pass Filter; RDG, Reflective Diffraction Grating; M, Mirror; PMFA, Polarization Maintaining Fiber Array; FS, Fiber Splitter; PM, Power Meter. b) SEM view of the multi-mode ring resonator.

though the use of a single-mode structure would have the advantage of a lower effective area of the mode, Q factors reached with multi-mode structures[18] are higher, granting an increased conversion efficiency. In Fig.1.(b) a SEM view of the resonator structure is shown and the transmission spectra of the pump resonance is reported in Fig.2. A similar spectral behaviour is observed for the signal and idler resonances. The ring was close to critical coupling condition with a loaded Q of ∼7400, corresponding to a propagation loss of $36.6dB/cm$. For this reason we used the un-approximated model to describe the FWM process[2], in which the FWM conversion efficiency η is defined as

$$\eta = \frac{P_i}{P_s} = |\gamma P_p L'|^2 \, FE_p^4 \, FE_s^2 \, FE_i^2 \tag{4}$$

$$L'^2 = L^2 \exp(-\alpha L) \left| \frac{1 - \exp(-\alpha L + j\Delta k L)}{-\alpha L + j\Delta k L} \right|^2 \tag{5}$$

where L' is the effective length and FE_j is the field enhancement (Eq.2) for the pump, signal and idler, respectively. With $P_{i/s}$ are identified the powers of the idler and signal, respectively. In Eq.5, the phase mismatch, due to the dispersion of the waveguide, is defined as follow

$$\Delta k = 2k_p - k_s - k_i \tag{6}$$

By performing the linear characterization of the sample[20], we retrieved a FE of 4.37 for the pump and signal, meanwhile we calculated a reduced value of 4.27 at the idler spectral position. Even though the wavelengths of the signal, idler and pump met three successive resonances of the cavity, the phase mismatch accumulated in the $\sim 26nm$ bandwidth caused the difference in FE value for the idler (see Supplementary Material for the dispersion and group index of the structure).

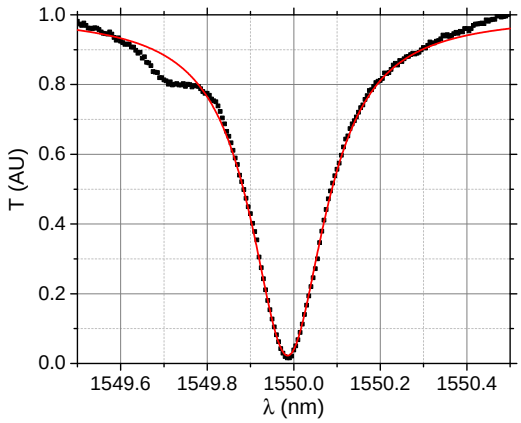

FIG. 2. Transmission spectrum of the pump resonance.

The experimental setup used for the characterization of the FWM process is depicted in Fig.1.(a) where the pump ($1549.99nm$) and signal ($1563.42nm$) were coupled in the same polarization maintaining fiber using a reflective diffraction grating, additionally providing more than $-45dB$ noise reduction at the idler frequency($1537.06nm$). The pump power was controlled by a Pritel polarization maintaining erbium-doped fiber amplifier, whose excess noise was attenuated using an additional band pass filter. The combined pump and signal waves were injected in the TE mode of the SiC waveg-

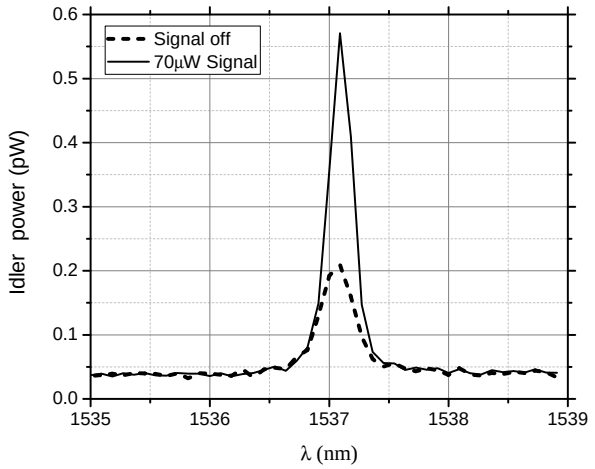

FIG. 3. Spectrum of the generated light at the idler wavelength for $1.2mW$ of on-resonance pump power with and without $70\mu W$ of signal input (black and dashed curves, respectively).

uide using a polarization maintaining fiber array polished at 8 degrees and apodized grating couplers optimized to achieve $> -7dB$ coupling efficiency[18]. In the output, the pump and signal were attenuated by the spectrometer and a band pass filter, meanwhile the generated idler intensity was measured with an InGaAs CCD array. A power meter was used to guarantee that the pump and signal were resonant with the ring resonator during the experiment, by minimizing the transmission. This also compensated the power dependent wavelength shift of the resonances given by thermo-optical and Kerr effects[8].

For a pump power of $1.2mW$ in the input waveguide, the measured idler power at the ring position is reported in Fig.3. The black curve represents the idler power measured at the ring for the stimulated case, with both signal ($70\mu W$) and pump on resonance, meanwhile the dashed curve was measured in the spontaneous case, with the signal laser switched off and the pump on resonance. In the spectral region outside the idler resonance of the ring (Fig.3), the power measured from the CCD is negligible as well as in the condition where the pump was off-resonance, ensuring that any influence of the EDFA noise is suppressed and to confirm that both stimulated and spontaneous signals are generated inside the ring. To establish the origin of the spontaneous signal (SpS) generated inside the resonator and extract the non-linear properties of the SiC waveguide, a pump power dependence measurement was performed. As depicted in the optical micrograph in Fig.1.(a), the sample is composed of a waveguide that couples to eight ring resonators with different radii, each corresponding to a different resonant frequency. This was made to overcome fabrication tolerances and deliver one ring with a resonance within the wavelength tuning range of the pump laser ($\sim 1.5nm$). In order to determine exactly the losses β between the fiber array and the ring used for frequency conversion,

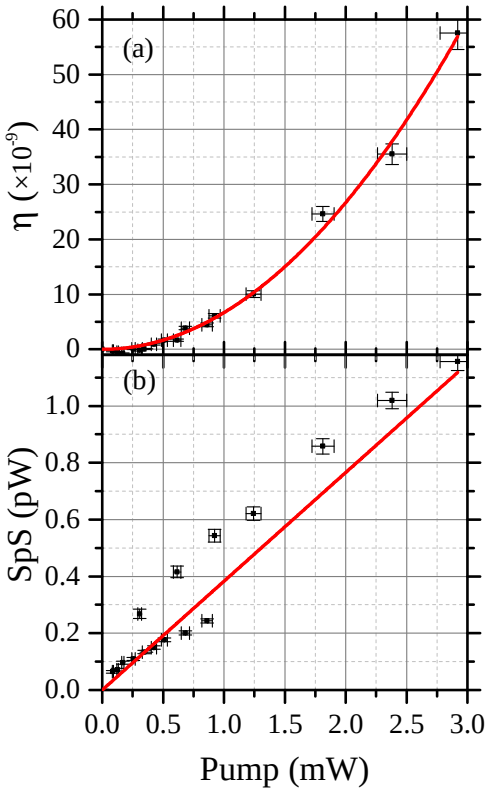

FIG. 4. a) Experimental FWM gain (black points) and quadratic fit (red line). b) Linear signal generated in the ring resonator versus resonant pump power (black points) and linear fit (red line).

we performed the experiment twice by inverting the input and output ports of the fiber array. With reference to Fig.1.(a), the pump injected in the sample through the Port 1 (Port2) of the fiber array was attenuated by a factor β_1 (β_2) at the ring position and corresponded to the FWM efficiency η_1 (η_2). Considering T the total transmission between Port 1 and Port 2, and from Eq.4

$$\eta_1/\eta_2 = (\beta_1/\beta_2)^2 \tag{7}$$

$$T = \beta_1\beta_2 \tag{8}$$

we retrieved the input loss values of $-12.61dB$ and $-6.99dB$. This difference in losses between the two experiments are attributed to propagation losses and imperfections deriving from the fabrication process.

The data points of the two experiments are combined in Fig.4 by taking in to account the extracted β_i values. The FWM gain for different pump powers is reported in Fig.4.(a) where the corresponding values of the generated SpS (Fig.4.b) were subtracted. By fitting Fig.4.(a) with the nonlinear gain of Eq.4, we retrieved the nonlinearity of the structure $\gamma = 3.86 \pm 0.03 W^{-1}m^{-1}$. The nonlinear

susceptibility can be estimated from Eq.1, in which[21]

$$A_{eff} = A_{NL} \iint_{-\infty}^{\infty} S_z \, dxdy \Big/ \iint_{NL} S_z \, dxdy \quad (9)$$

with A_{NL} the area of the waveguide cross-section and S_z is the Poynting vector parallel to the propagation direction. The absence of a cladding able to participate to the FWM process is accounted in Eq.9, where only the power flow in the nonlinear (NL) SiC cross-section is integrated in the denominator. Using a mode solver, we calculate $A_{eff} = 0.558(\mu m)^2$, corresponding to $n_2 = (5.31 \pm 0.04) \times 10^{-19} m^2/W$. This value is in partial agreement with the estimated value for bulk crystalline SiC[17] of $4.87 \times 10^{-19} m^2/W$.

The SpS generated without signal input is shown in Fig.4.(b) and is fitted using a linear dependence with the pump power. A possible explanation for this signal is provided by Raman scattering, even if in crystalline 3C SiC, Raman signals due to the main optical phonon modes[22] are expected at $\sim 200nm$ away from the pump wavelength. It is possible that the high density of crystalline defects at the SiC-Si interface[23] might introduce a complex continuous spectrum that can benefit of the FE in the resonator and generate this spontaneous field. From the fit to the experimental data we estimated this linear component to have a gain in the ring of $(3.8 \pm 0.3) \times 10^{-10}$. The presence of this gain could provide an explanation to the fact that the measured value of n_2 is higher than the calculated nonresonant value[17]. Low energy measurements of heteroepitaxially-grown SiC thin films could provide more information on the origin of the linear signal, an in-depth analysis of this effect is left for future works.

In conclusion, we demonstrated frequency conversion in a 3C SiC ring resonator. The tight confinement provided a high nonlinearity of the structure of $3.86 W^{-1} m^{-1}$ while the use of the small radius ring resonator enhanced the nonlinear gain of $\sim 50dB$ compared to a straight waveguide of the same length[2]. As reported in Ref.[18], the quality factor of SiC ring resonators can be increased by further optimization of the fabrication process and therefore the nonlinear performances can be improved. This demonstration is an essential step in the development of 3C SiC nonlinear photonic and shows the potential of this platform.

SUPPLEMENTARY MATERIAL

See Supplementary Material for the linear optical characterization of the ring resonator.

FUNDING INFORMATION

This work was supported by the Engineering and Physical Sciences Research Council (EPSRC) EP/P003710/1.

ACKNOWLEDGMENTS

We acknowledge support from the Southampton Nanofabrication Centre and experimental support by Otto Muskens.

[1] A. C. Turner, M. A. Foster, A. L. Gaeta, and M. Lipson, "Ultra-low power parametric frequency conversion in a silicon microring resonator," Opt. Express **16**, 4881–4887 (2008).

[2] P. P. Absil, J. V. Hryniewicz, B. E. Little, P. S. Cho, R. A. Wilson, L. G. Joneckis, and P.-T. Ho, "Wavelength conversion in gaas micro-ring resonators," Opt. Lett. **25**, 554–556 (2000).

[3] M. A. Foster, A. C. Turner, R. Salem, M. Lipson, and A. L. Gaeta, "Broad-band continuous-wave parametric wavelength conversion in silicon nanowaveguides," Opt. Express **15**, 12949–12958 (2007).

[4] M. A. Foster, A. C. Turner, J. E. Sharping, B. S. Schmidt, M. Lipson, and A. L. Gaeta, "Broad-band optical parametric gain on a silicon photonic chip," Nature **441**, 960–963 (2006).

[5] R. H. Stolen and C. Lin, "Self-phase-modulation in silica optical fibers," Phys. Rev. A **17**, 1448–1453 (1978).

[6] S. Azzini, D. Grassani, M. Galli, D. Gerace, M. Patrini, M. Liscidini, P. Velha, and D. Bajoni, "Stimulated and spontaneous four-wave mixing in silicon-on-insulator coupled photonic wire nano-cavities," Applied Physics Letters **103**, 031117 (2013).

[7] J. Leuthold, C. Koos, and W. Freude, "Nonlinear silicon photonics," Nature Photonics **4**, 535 (2010).

[8] J. S. Levy, A. Gondarenko, M. a. Foster, A. C. Turner-Foster, A. L. Gaeta, and M. Lipson, "CMOS-compatible multiple-wavelength oscillator for on-chip optical interconnects," Nature Photonics **4**, 37–40 (2009).

[9] H. Jung, C. Xiong, K. Y. Fong, X. Zhang, and H. X. Tang, "Optical frequency comb generation from aluminum nitride microring resonator," Opt. Lett. **38**, 2810–2813 (2013).

[10] B. J. M. Hausmann, I. Bulu, V. Venkataraman, P. Deotare, and M. Lončar, "Diamond nonlinear photonics," Nature Photonics **8**, 369–374 (2014).

[11] J. L. O'Brien, A. Furusawa, and J. Vučković, "Photonic quantum technologies," Nature Photonics **3**, 687–695 (2009).

[12] G. Calusine, A. Politi, and D. D. Awschalom, "Silicon carbide photonic crystal cavities with integrated color centers," Applied Physics Letters **105**, 011123 (2014).

[13] S. Yamada, B.-S. Song, S. Jeon, J. Upham, Y. Tanaka, T. Asano, and S. Noda, "Second-harmonic generation in a silicon-carbide-based photonic crystal nanocavity." Optics letters **39**, 1768–71 (2014).

[14] C.-H. Cheng, C.-L. Wu, Y.-H. Lin, W.-L. Yan, M.-H. Shih, J.-H. Chang, C.-I. Wu, C.-K. Lee, and G.-R. Lin, "Strong optical nonlinearity of the nonstoichiometric silicon carbide," J. Mater. Chem. C **3**, 10164–10176 (2015).

[15] X. Lu, J. Y. Lee, S. Rogers, and Q. Lin, "Optical kerr nonlinearity in a high-q silicon carbide microresonator," Opt. Express **22**, 30826–30832 (2014).

[16] J. Cardenas, M. Yu, Y. Okawachi, C. B. Poitras, R. K. Lau, A. Dutt, A. L. Gaeta, and M. Lipson, "Optical nonlinearities in high-confinement silicon carbide waveguides," Optics letters **40**, 4138–4141 (2015).

[17] F. De Leonardis, R. A. Soref, and V. M. Passaro, "Dispersion of nonresonant third-order nonlinearities in silicon carbide," Scientific reports **7**, 40924 (2017).

[18] F. Martini and A. Politi, "Linear integrated optics in 3c silicon carbide," Opt. Express **25**, 10735–10742 (2017).

[19] M. A. Foster, A. C. Turner, M. Lipson, and A. L. Gaeta, "Nonlinear optics in photonic nanowires," Optics Express **16**, 1300 (2008).

[20] P. Rabiei, W. Steier, C. Zhang, and L. Dalton, "Polymer microring filters and modulators," Journal of Lightwave Technology **20**, 1968–1975 (2002).

[21]I. D. Rukhlenko, M. Premaratne, and G. P. Agrawal, "Effective mode area and its optimization in silicon-nanocrystal waveguides," Opt. Lett. **37**, 2295–2297 (2012).

[22]K. Karch, P. Pavone, W. Windl, O. Schütt, and D. Strauch, "Ab initio," Phys. Rev. B **50**, 17054–17063 (1994).

[23]R. Anzalone, G. D'arrigo, M. Camarda, C. Locke, S. Saddow, and F. La Via, "Advanced residual stress analysis and fem simulation on heteroepitaxial 3c–sic for mems application," Journal of Microelectromechanical Systems **20**, 745–752 (2011).